Nitrogen-related dopant and defect states in CVD diamond

E. Rohrer, C. F. O. Graeff, R. Janssen, C. E. Nebel, and M. Stutzmann
Walter Schottky Institut, Technische Universität München, Am Coulombwall, D-85748 Garching, Germany

H. Güttler and R. Zachai
Materials Research, Daimler Benz AG, D-89013 Ulm, Germany

(Received 31 October 1995; revised manuscript received 11 April 1996)

Subbandgap absorption of chemical-vapor-deposition diamond films, with nitrogen contents varying from 10 to 132 ppm has been explored by the constant-photoconductivity method (CPM), photothermal-deflection spectroscopy (PDS) and electron spin resonance (ESR). The spectra measured by PDS increase monotonically and are structureless with increasing photon energies indicating absorption due to amorphous carbon and graphite. The CPM data show distinct features, with absorption bands at $h\nu = 1.6$, 4.0, and 4.7 eV in the nominally undoped film, and 2.4 and 4.7 eV in nitrogen-rich layers respectively. The CPM spectra of the doped films are comparable to photoconductivity data of synthetic Ib diamond. The defect densities involved increase with increasing nitrogen content. From ESR, a vacancy-related defect density ($g = 2.0028$) is deduced. Paramagnetic nitrogen ($g = 2.0024$) can be detected in the high-quality CVD layer or by illuminating the nitrogen-rich samples with photon energies larger than the band gap. [S0163-1829(96)09535-5]

I. INTRODUCTION

The unique properties of diamond have attracted considerable interest, especially after the discovery that low-cost and large-area diamond films can be grown by the chemical-vapor-deposition (CVD) technique.[1,2,3] Presently, one of the main applications of CVD diamond is as a substrate for high-power electronics due to its excellent thermal conductivity. Recent improvement of film quality suggests that active electronic devices for high-temperature or high-power operation can be realized in the near future. However, a variety of problems still have to be solved. Due to the microcrystalline structure of CVD diamond, grain boundaries, and surface and bulk defect states dominate the optical and electronic properties. Especially amorphous and graphitic carbon at surfaces and interfaces affect the dark conductivity as well as the optical absorption. Spectroscopy of bulk defect states, regarding their distributions and densities in the band gap, is therefore difficult and data available in the literature is still limited.

N-type doping has up to now not been understood. Nitrogen is a possible donor in diamond with lower formation energy than phosphorus.[4,5] Experiments with synthetic and natural diamond, however, show that in addition to the deep donor level at 1.7 eV (Ref. 29) below the conduction band, a variety of nitrogen-related defects are created that dominate transport and recombination of carriers. For successful production of electronic garde material, exploration of nitrogen-related effects is important. Excellent techniques for the investigation of band-gap states are photothermal-deflection spectroscopy (PDS) and the constant-photocurrent method (CPM).[6,7] PDS experiments detect spectrally resolved states that absorb light, while CPM is sensitive to absorption events that generate mobile carriers. CPM is therefore much less sensitive to surface than to bulk absorption. The application of both techniques then allows us a study of both surface and bulk defect densities. For an investigation of nitrogen-related doping and defect effects, electron-spin-resonance (ESR) experiments have also been applied. A series of CVD diamond films with nitrogen content varying between 10 and 132 ppm will be discussed in the following.

II. EXPERIMENT

The diamond films were grown at $T = 750$ °C on silicon in a standard CVD system described in Ref. 8, using H_2 and CH_4 as the main gas sources. To study the effect of nitrogen on the film properties, the nitrogen content in the gas phase was varied from 0 to 4% N_2/CH_4. Elastic-recoil-detection experiments[9] show that these films contain 10–132 ppm nitrogen (see Table I). The intentionally doped films show neither oriented nor textured crystal growth and appear nearly black in color. Sample thicknesses varied between 7 and 9 μm. Even the nominally undoped sample had 10 ppm nitrogen in the layer of thickness $d = 55$ μm. This diamond film is highly oriented, (100) textured with typical 10-μm grain size.

Photoconductivity measurements with planar contacts on top of the diamond sample (coplanar contact configuration), photothermal-deflection spectroscopy, and electron-spin-resonance measurements were performed using free-standing

TABLE I. Nitrogen content in the gas phase compared to the fraction incorporated in the diamond film measured by ERD (Ref. 9).

N_2/CH_4 (%)	N/C (ppm)
0	10
0.3	25
1.13	35
2.67	100
4	132

diamond films, where the silicon substrate had been removed by a KOH etching process.

The CPM experiments were performed either in coplanar or in sandwich contact configuration. For the coplanar configuration, two barlike Ti/Pt/Au contacts 1 mm apart were evaporated on top of the diamond films. Sandwich geometry was realized using the silicon substrate as back electrode and a semitransparent Ti/Pt/Au top contact 1 mm in diameter. As light sources, a halogen, a xenon, and a deuterium lamp were used. The light was dispersed in a Spex 340E monochromator using three different gratings blazed at 1000, 500, and 250 nm, respectively, and was mechanically chopped at 2 Hz. All optical parts employed, including the vacuum chamber window, have optical transparency up to 200 nm. The signal was detected via a lock-in amplifier. The light intensity was measured with a pyroelectric detector.

For transport measurements, the samples were mounted in a vacuum chamber with $p<10^{-6}$ mbar. To remove water and other contaminants from the surface, a heat treatment at 500 K for 30 min was used. All CPM, PDS, and ESR data were measured at room temperature.

CPM experiments performed in sandwich contact configuration offer several advantages compared to the conventional coplanar contact geometry. (1) In the high-quality CVD diamond films with columnar structure, the photogenerated carriers propagate in the crystals and do not have to cross grain boundary barriers. (2) Much higher electric fields can be applied than in coplanar structures. (3) Thin layers on Si substrates can be investigated without the problems involved in the characterization of free-standing films.

In the following, we briefly summarize the basic assumptions of CPM. With a constant quantum efficiency η, uniform illumination throughout the film thickness d, and a photocurrent dominated by unipolar properties over the whole spectral range, the photocurrent density j_{ph} is given by

$$j_{\mathrm{ph}}=en\mu V/d, \tag{1}$$

where V is the applied voltage, e the elementary charge, and μ the carrier mobility. For monomolecular recombination, the carrier density n is given by the product of lifetime τ and the generation rate g:

$$n=\tau g=\tau\eta\Phi(1-R)[1-\exp(-\alpha d)]1/d, \tag{2}$$

where Φ is the photon flux, R the reflectivity, and α the absorption coefficient. For $\alpha d\ll 1$, the photocurrent is

$$j_{\mathrm{ph}}=e\mu\tau\eta\Phi(1-R)\alpha V/d. \tag{3}$$

By keeping the photocurrent constant, the quasi-Fermi-level position and therefore the occupation of defects in the gap remains unchanged over the entire spectral range. In this case, the lifetime τ is constant and the absorption coefficient α can be expressed by (see Ref. 7 for example)

$$\alpha(h\nu)=\frac{\text{const.}}{\Phi(h\nu)}, \tag{4}$$

neglecting any energy dependence of the reflectivity.

For photothermal deflection spectroscopy,[10] the free-standing CVD diamond films were attached to a quartz holder, which was immersed in spectroscopically pure C_6F_{14}. ESR experiments on free-standing samples were performed in the TE_{102} cavity of a standard X-band ESR spectrometer using 100-kHz magnetic-field modulation. For light-induced ESR (LESR) experiments the samples were illuminated with a Hg/Xe arc lamp.

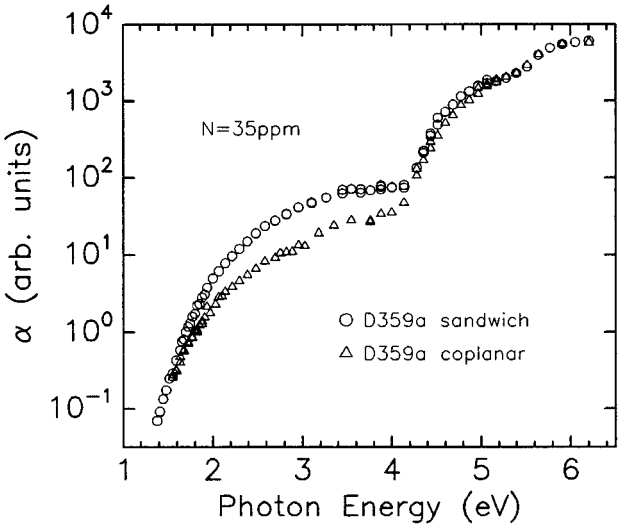

FIG. 1. CPM spectra of a CVD diamond film with different contact geometries.

III. EXPERIMENT RESULTS

Sub-band-gap photocurrent studies of CVD diamond are at present subject to a controversy concerning the role of internal photoemission over contact barriers. While Okumura, Mort, and Machonkin[11] demonstrated that internal photoemission is negligible compared to the absorption of the CVD diamond layer, Hicks *et al.*[12] attribute the absorption predominantly to internal photoemission. The conflicting findings may be partly due to different film qualities. It is very likely that for a strongly absorbing CVD diamond film, internal photoemission is a negligible effect, whereas for layers with small sub-band-gap absorption, the opposite is the case. To investigate in our case whether or not internal photoemission is negligible, we have performed CPM experiments in coplanar and sandwich contact geometry. In coplanar contact configuration, thick metal contacts were used and the samples were illuminated only between the electrodes so that internal photoemission should be negligible.

Figure 1 shows a typical result. The sample is nitrogen rich, containing 35 ppm nitrogen, and is 77 μm thick. The absorption spectra in the energy range $E>4.5$ eV are comparable for both contact geometries. For lower photon energies the CPM in sandwich geometry gives a slightly higher (factor of 3) absorption. The onset of the absorption at $E>1.4$ eV indicates a Fermi-level position, which is at least 1.4 eV away from the conduction-band edge. Internal photoemission should contribute most strongly in this absorption regime and the differences in absorption should be largest. The two spectra, however, approach each other. We conclude, therefore, that in both cases the absorption is governed by transitions in the diamond film. The difference is attributed to a difference in film quality, since CVD diamond films exhibit a pronounced lateral inhomogeneity. In the follow-

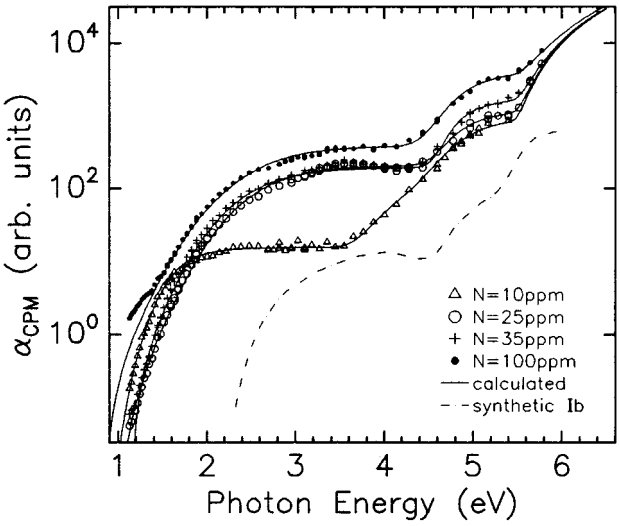

FIG. 2. CPM spectra of CVD diamond films compared with a photoconductivity spectrum of a synthetic Ib diamond (Ref. 24) drawn in arbitrarily. The full lines are the calculated fits to the data.

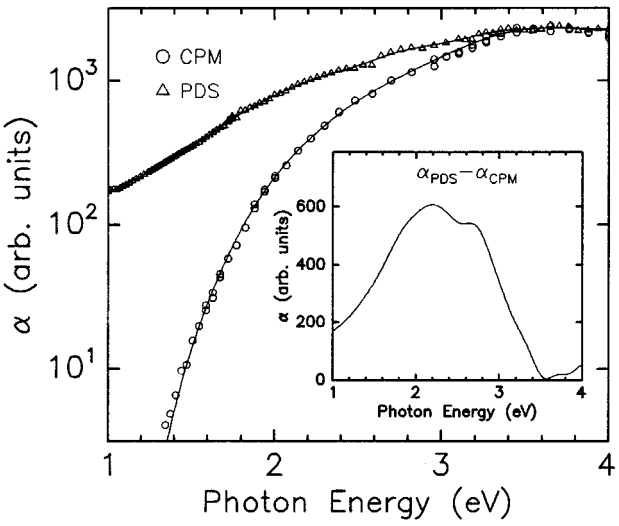

FIG. 4. CPM and PDS spectra of a CVD diamond film containing 35 ppm nitrogen. The inset shows the difference between α_{PDS} and α_{CPM} in linear scale.

ing, we therefore neglect contributions of internal photoemission.

Figure 2 shows CPM spectra of three heavily nitrogen-doped samples, containing 25, 35, and 100 ppm nitrogen, and of the nominally undoped diamond film with 10 ppm nitrogen. The CPM spectra reveal distinct features in absorption of CVD diamond films. The increase in nitrogen causes an overall increase in sub-band-gap absorption and a variation in the shape of the absorption spectra. The ''intrinsic'' layer shows an onset of absorption at photon energies $E>1$ eV approaching an absorption plateau in the range 2–3.6 eV, then increasing towards a second plateau at $E\approx 5$ eV, where the absorption further increases due to increasing contributions of band-to-band transitions. The nitrogen-rich films show stronger absorption, increasing in the range 1.2–3.5 eV, with a plateau at $E\approx 5$ eV and a further increase due to band-to-band transitions. A detailed discussion of these features will be given in Sec. IV.

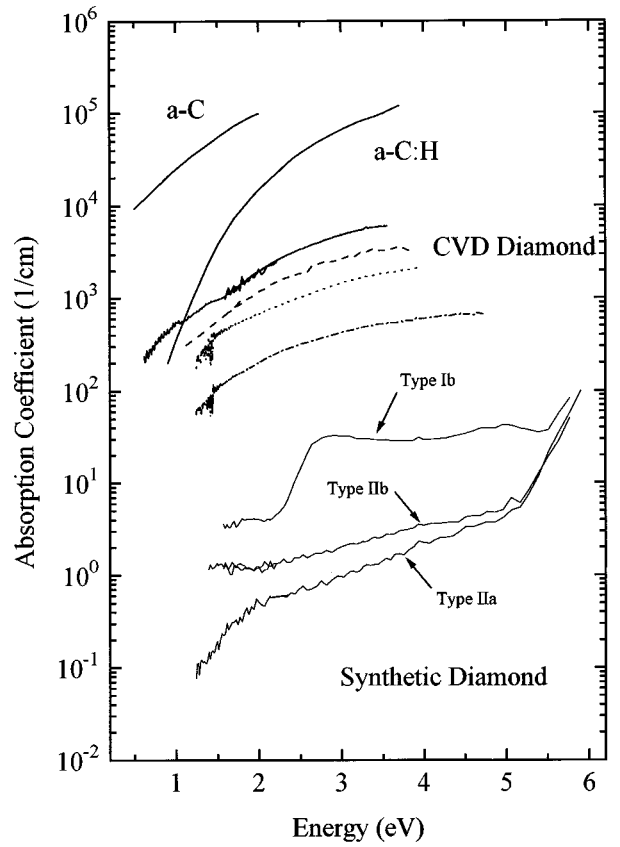

FIG. 3. Absorption spectra of a-C and a-C:H (Refs. 13, 14) and PDS measurements of synthetic and CVD diamond. —: $d=7.2$ μm, $N=132$ ppm. ---: $d=7.4$ μm, $N=25$ ppm. ⋯: $d=15.8$ μm, $N=10$ ppm. -·-·-: $d=77.2$ μm, $N=35$ ppm.

Results of the PDS experiments are shown in Fig. 3, including data obtained on Ib, IIa, and IIb synthetic diamond. Absorption spectra of amorphous carbon and of hydrogenated amorphous carbon from Refs. 13 and 14 are also depicted for comparison. For all CVD diamond samples investigated, the PDS absorption increases continuously toward higher photon energies. With increasing nitrogen content, an overall increase in absorption is detected. Layers with larger thickness absorb less due to the improving quality of CVD diamond films with increasing layer thickness. On the average, the absorption coefficient of the CVD diamond films is approximately a factor 500 larger than that of synthetic diamond and shows no comparable spectral dependence. The spectral-absorption variation of the CVD diamond films is comparable to the increase in absorption in amorphous carbon films despite the fact that it is about 1–2 orders of magnitude smaller. In Fig. 4, a comparison of PDS and CPM data is shown. The data have been normalized in an arbitrary way at 4 eV to demonstrate the spectral differences at lower energies. The inset shows the difference between PDS and CPM spectra on a linear scale. In the energy range $E<3$ eV, the PDS spectrum is much less energy dependent than CPM. Optical microscopy clearly indicates that the strongly absorbing regions are at the surface of the crystallites. This points toward amorphous and/or graphitic layers at surfaces

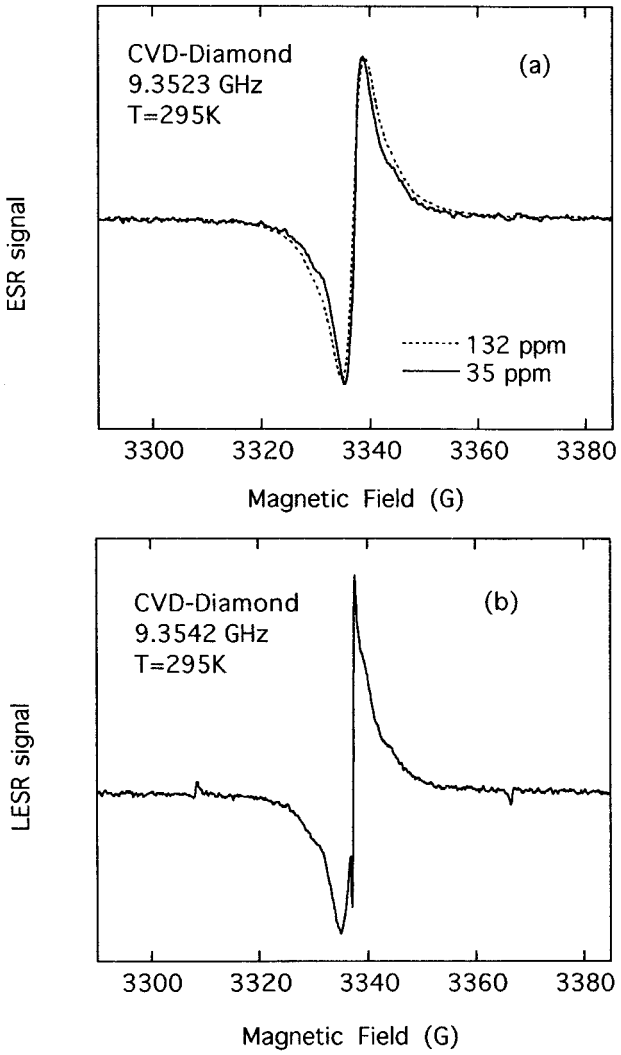

FIG. 5. (a) Typical ESR signals of two CVD diamond films containing 35 and 132 ppm nitrogen, respectively. (b) LESR signal of a CVD diamond film containing 35 ppm nitrogen.

and grain boundaries, which dominate optical-absorption experiments such as PDS, a conclusion also drawn by Nesládek *et al.*[15]

In Fig. 5, typical ESR and LESR spectra are shown. ESR studies of CVD diamond films have shown both substitutional nitrogen[16] and vacancy-related defects.[17] In our case, we have observed the resonance related to the latter, with a $\Delta H_{pp} \approx 4G$ and $g = 2.0028$. Note that the signal consists of a single central line with unresolved shoulders. The presence of these shoulders was first attributed to two overlapping lines, one narrow and one broad, which have essentially the same g value.[17] More recently, the signal has been described as a central line and two hyperfine satellites related to nearby hydrogen nuclei.[18,19] The substitutional N-donor-related resonance could be detected on the high-quality CVD layer with 10 ppm nitrogen. On samples with higher N content, the resonance could only be observed under illumination with band-gap UV light [LESR, see Fig. 5(b)]. From studies on natural and synthetic diamond, it is known that nitrogen is the dominant impurity, with many forms from isolated substitutional and paramagnetic to several nonparamagnetic aggregates. The substitutional form is a deep donor with a level at 1.7 eV below the conduction band, giving rise to the well established ESR signal with a g value of 2.0024 and a triplet hyperfine structure due to the interaction with the ^{14}N nuclear spin. It saturates at relatively low microwave powers owing to the long relaxation time. In other configurations it is a dominant optical-absorption center, distributed in the band gap, forming aggregates and structural defects that compensate the isolated substitutional nitrogen.

IV. DISCUSSION

In this section we discuss the experimental results in order to identify defects dominating the sub-band-gap absorption as detected by CPM and PDS.

The absorption measured by PDS is only weakly increasing over approximately one order of magnitude towards higher energies, showing no specific structure. Nesládek *et al.*[15] attribute this to $\pi - \pi^*$ band-type transitions in amorphous carbon.[20,21] Close similarity to a-C is obvious only in the spectral range 1–2 eV (see Fig. 3). The slightly weaker variation of the absorption is most likely caused by the presence of graphitic clusters at grain boundaries and surface parts. This argument is supported by micrographs (not shown here) taken by an optical microscope in transmission mode. The grain boundaries are dark and strongly absorbing, whereas the centers of the (100)-oriented grains are bright and transparent.[22]

The bulk absorption of CVD diamond, detected by CPM, is comparable to the absorption of nitrogen-rich synthetic diamond,[23] indicating the close similarity between both types of materials. Taking into account data available in the literature, it is well known that optical absorption, centered at 4.6 eV, is correlated with isolated paramagnetic nitrogen.[24] A continuum absorption starting at 4 eV and extending to higher energy has been attributed to A centers (a substitutional nitrogen pair at adjacent sites).[25,26] The small dip around 4.5 eV points toward an absorption process that is competitive with transitions leading to a photocurrent.[23] The absorption in the energy range 1.2–3.5 eV has been ascribed to nitrogen donor excitations into the conduction band.[27–29] All these defects are more-or-less present in the nitrogen-rich samples.

The sample containing 10 ppm nitrogen shows some different features. The onset of the photocurrent at approximately 1 eV turns into a plateau at about 2 eV, rising at 3.6 eV toward a plateau at 5 eV, and finally increases due to band-to-band transitions. A strong paramagnetic nitrogen resonance is detectable in this layer, indicating that at least a fraction of the incorporated nitrogen is electronically active as dopant. The nitrogen dopant level is 1.7 eV below the conduction band,[28] which agrees rather well with the detected onset of absorption. The increase in absorption in the energy range >3.6 eV can be due to different nitrogen aggregates, as described above.

To determine the energy levels and distributions of defects more precisely, the spectra have been deconvoluted based on the assumption that electrons dominate transport. With $N_i(\epsilon)$ the initial, $N_f(\epsilon)$ the final density of state and $f(\epsilon)$ being the Fermi-Dirac distribution function, the absorption coefficient $\alpha(h\nu)$ can be calculated assuming a constant matrix element and neglecting any energy dependence of the index of refraction[30]:

TABLE II. Energy levels, distributions, and densities of defects in the nominally undoped film containing 10 ppm nitrogen.

$h\nu$ (eV)	FWHM (eV)	Defect density (arb. units)
1.6±0.15	0.4 ±0.1	0.55±0.05
4.0±0.15	0.45±0.1	7±0.5
4.7±0.15	0.5 ±0.1	65±5

$$\alpha(h\nu)=\frac{\text{const.}}{h\nu}\int N_i(\epsilon)f(\epsilon)N_f(\epsilon+h\nu)[1-f(\epsilon+h\nu)]d\epsilon. \tag{5}$$

The Fermi energy E_F separates occupied and empty states, leading to

$$\alpha(h\nu)=\frac{\text{const.}}{h\nu}\int_{E_F-h\nu}^{E_F} N_i(\epsilon)N_f(\epsilon+h\nu)d\epsilon. \tag{6}$$

Since diamond is an indirect semiconductor, the absorption coefficients of transitions with phonon emission and phonon absorption must be summed:

$$\alpha(h\nu)=\alpha_{\text{em}}(h\nu)+\alpha_{\text{abs}}(h\nu). \tag{7}$$

The defect distributions are supposed to be Gaussian:

$$N_i^{\text{def}}(\epsilon)=\sum_j \frac{A_j}{\sqrt{2\pi}W_j}\exp\left(-\frac{(\epsilon-E_{Gj})^2}{2W_j^2}\right), \tag{8}$$

with the defect center energy E_{Gj}, the full width at half maximum (FWHM) $2W_j$, and the defect density A_j. The valence and conduction bands are assumed to be parabolic:

$$N_i^{\text{vb}}(\epsilon)=N_v\sqrt{-(\epsilon-e_0)}, \tag{9}$$

$$N_f^{\text{cb}}(\epsilon+h\nu)=N_c\sqrt{\epsilon+h\nu-E_{\text{gap}}\pm E_{\text{phonon}}+e_0}. \tag{10}$$

N_f^{cb} has to be multiplied by f_{BE} in the case of phonon absorption and by $f_{\text{BE}}+1$ for phonon emission, f_{BE} being the Bose-Einstein distribution function. The parameter e_0 (Ref. 31) was introduced to obtain an effective density of states at the band edges:

$$N_v\sqrt{e_0}=N_c\sqrt{e_0}=\text{const.} \tag{11}$$

Since $\alpha(h\nu)$ is in arbitrary units, the CPM spectra of different samples are matched by the calculations assuming the same effective density of states at the band edges in all samples. This effective density of states is unknown, so that the calculated defect densities are in arbitrary units. An experimental normalization of the absolute CPM absorption coefficient, for example by transmission/reflection experiments, is prevented by light-scattering effects at grain boundaries and by absorption of graphitic or amorphous carbon (see the comparison between CPM and PDS).

Three absorption centers are deduced for the sample containing 10 ppm nitrogen with energy levels at 1.6, 4.0, and 4.7 eV below the conduction band. The spectra of the nitrogen-rich samples are fitted with two Gaussian defect distributions around 2.5 and 4.7 eV below the conduction-band edge. Details are summarized in Tables II and III.

TABLE III. Energy levels, distributions, and densities of defects in the intentionally nitrogen-doped films.

N (ppm)	$h\nu$ (eV)	FWHM (eV)	Defect density (arb. units)
25	2.5±0.15	0.8±0.1	9.3±0.5
	4.7±0.15	0.35±0.1	80±5
35	2.4±0.15	0.8±0.1	8.5±0.5
	4.7±0.15	0.27±0.1	130±50
100	2.4±0.15	0.9±0.1	17±5
	4.7±0.15	0.43±0.1	300±50

Figure 6 shows the variation of the defect density of the 4.7-eV defect center versus nitrogen content. The defect density of this center increases proportionally with nitrogen concentration. In the literature, the 4.65-eV center, which we assume is the same as our 4.7-eV defect, is linearly correlated with the paramagnetic nitrogen density. For the nitrogen-rich samples, the absolute density of paramagnetic nitrogen cannot be determined experimentally because the spin density falls below the detection limit of our system. Exposing the samples to UV light causes a significant increase of the spin density related to substitutional nitrogen. An absolute evaluation, however, is difficult, because the absorption of UV light is inhomogeneously distributed in the diamond layer, and the active area, where the spins are generated, is not accurately known. Obviously, a charge transfer from the fourfold-coordinated nitrogen (dopant) atoms to deep defects takes place, leaving most of the nitrogen dopants empty. By UV light exposure, the nitrogen dopants are populated by optically excited electrons and become paramagnetic. Figure 7 shows the defect variation ($g=2.0028$, vacancy related) versus nitrogen content. The absolute nitrogen densities have been calculated by taking into account the density of diamond which is 1.76×10^{23} cm^{-3}. The increase in defect density scales with the increase in nitrogen, indicating that each nitrogen atom, which is incorporated into the host lattice of the diamond, creates about one defect. In the sample with low nitrogen content (10 ppm$=1.76\times10^{18}$ cm^{-3}) 5×10^{16} cm^3 paramagnetic nitrogen can be detected without light exposure. Only a few percent of the incorporated nitrogen is paramagnetic. UV light causes an increase by a factor of 3 in the spin density. The onset of absorption

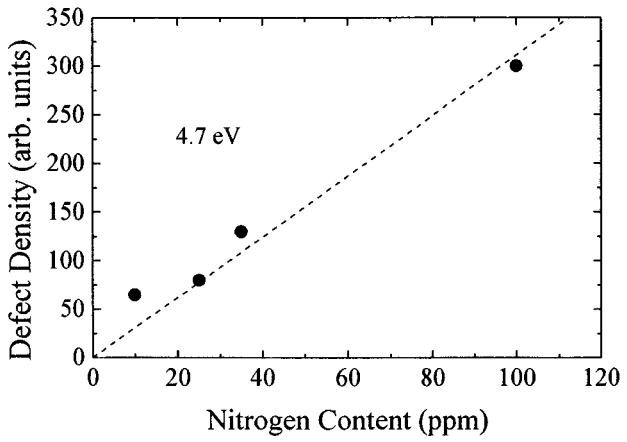

FIG. 6. Defect densities of the absorption band centered at 4.7 eV versus nitrogen content, derived from fits to CPM spectra.

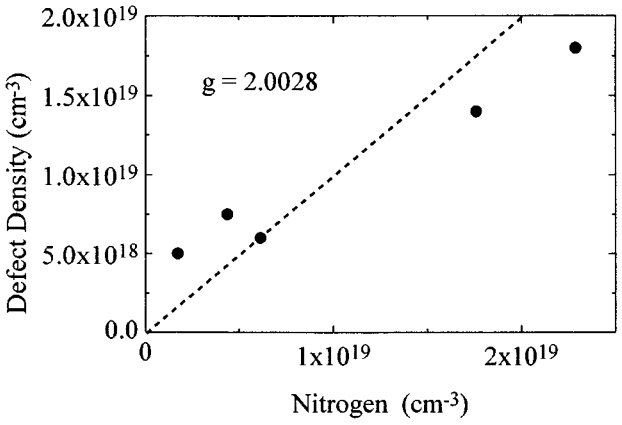

FIG. 7. Defect densities of vacancy-related defects ($g=2.0028$) determined by ESR.

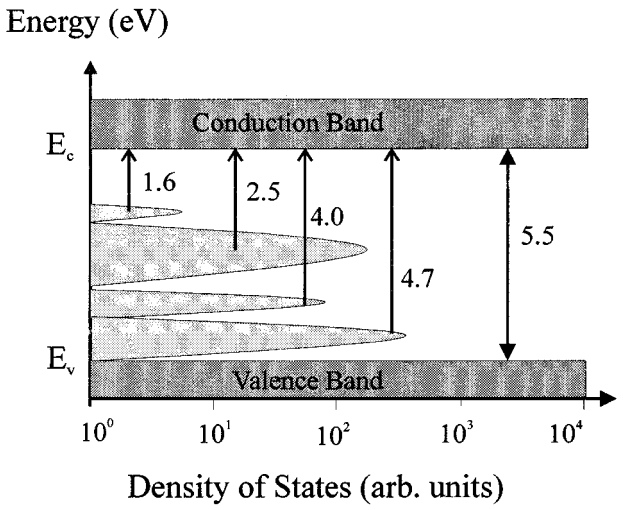

FIG. 8. Schematic energy diagram of the defects, determined by deconvolution of the CPM spectra.

in the CPM spectra indicate that the Fermi level is in the range <1.5 eV from the conduction band. If so, then the paramagnetic spin density represents approximately the density of nitrogen donors.

Figure 8 summarizes the energetic levels of the detected defects. The 1.6-eV level is attributed to the substitutional nitrogen donor level. The 2.5-eV level varies little with nitrogen content. Further investigations are needed to clarify the nature of this defect. The 4.7-eV defect niveau is strongly present in all samples and increases with increasing nitrogen content. A correlation with nitrogen is therefore obvious. However, the creation mechanism and the microscopic defect configuration are not clear. Finally, the 4.0-eV defect, which is attributed to the *A* center, can be detected only on the nominally undoped diamond film.

V. CONCLUSION

The investigation of CVD diamond films with PDS, CPM, and ESR reveal several features.

(1) PDS is dominated by surface and interface absorption centers, indicated by the featureless increase in absorption. This indicates a higher surface than bulk state density.

(2) Photoconductivity experiments give access to bulk properties. The sub-band-gap absorption of CVD films, containing nitrogen in the range 10–135 ppm, is comparable to synthetic diamond. The identification of the defects can be done based on data available in the literature. Variation of the nitrogen content, however, does not result in the expected variations in defect densities. This is most likely due to the polycrystalline nature of CVD diamond.

(3) ESR experiments have detected two resonances. The $g=2.0028$ resonance attributed to a vacancy-related defect is present in all samples under investigation. A linear increase with nitrogen content is detected, indicating that each nitrogen atom which is incorporated creates about one defect. The $g=2.0024$ resonance, which is due to paramagnetic nitrogen, can be detected only in samples with less then 20 ppm nitrogen. Here, only 1% of the total nitrogen is paramagnetic. In samples with higher nitrogen concentrations, this g value can be detected only under UV illumination, indicating that the nitrogen donors are empty, and that the Fermi level is below the nitrogen donor level. Light exposure causes a filling of these states, at least partially.

ACKNOWLEDGMENTS

This work has been supported by the B.M.B.F. under Contract No. 3N1001G4. C.F.O.G. is pleased to acknowledge the Alexander von Humboldt Stiftung for partial financial support.

[1] B. V. Spitsyn, L. L. Bouilov, and B. V. Derjaguin, J. Cryst. Growth **52**, 219 (1981).
[2] S. Matsumoto, Y. Sato, M. Kamo, and N. Setaka, Jpn. J. Appl. Phys. **21**, L183 (1982).
[3] A. Sawabe and T. Inuzuka, Thin Solid Films **137**, 89 (1986).
[4] A. B. Anderson and S. P. Mehandra, Phys. Rev. B **48**, 4423 (1993).
[5] S. A. Kajihara, A. Antonelli, and J. Bernholc, Physica B **185**, 144 (1993).
[6] H. G. Grimmeiss and L.-Å. Ledebo, J. Appl. Phys. **46**, 2155 (1975).
[7] M. Vaněček, A. Abrahám, O. Štika, J. Stuchlík and J. Kočka, Phys. Status Solidi A **83**, 617 (1984).
[8] H.-J. Füβer, M. Rosler, M. Hartweg, R. Zachai, X. Jiang, and C.-P. Klages, J. Electrochem. Soc. **93–17**, 102 (1993).
[9] A. Bergmaier, G. Dollinger, T. Faestermann, C. M. Frey, M. Ferguson, H. Güttler, G. Schulz, and H. Willerscheid (unpublished).
[10] W. Jackson, N. M. Amer, A. C. Boccara, and D. Fournier, Appl. Opt. **20**, 1333 (1981).
[11] K. Okumura, J. Mort, and M. A. Machonkin, Philos. Mag. Lett. **65**, 105 (1992).
[12] M. C. Hicks, C. R. Wronski, S. A. Grot, G. Sh Gildenblat, A. R. Badzian, T. Badzian, and R. Messier, J. Appl. Phys. **65**, 2139 (1989).
[13] J. J. Hauser, J. Non-Cryst. Solids **23**, 21 (1977).
[14] F. W. Smith, J. Appl. Phys. **55**, 764 (1984).

[15] M. Nesládek, M. Vaněček, and L. M. Stals, Phys. Status Solidi A **154**, 283 (1996).
[16] M. Hoinkis, E. R. Weber, M. I. Landstrass, M. A. Plano, S. Han, and D. R. Kania, Appl. Phys. Lett. **59**, 1870 (1991).
[17] M. Fanciulli and T. D. Moustakas, Phys. Rev. B **48**, 14 982 (1993).
[18] S. L. Holder, L. G. Rowan, and J. J. Krebs, Appl. Phys. Lett. **64**, 1091 (1994).
[19] X. Zhou, G. D. Watkins, and K. M. McNamara, Mater. Sci. Forum **196–201**, 825 (1995).
[20] J. Robertson and E. P. O'Reilly, Phys. Rev. B **35**, 2946 (1987).
[21] J. Robertson, Philos. Mag. B **66**, 199 (1992).
[22] C. E. Nebel, E. Rohrer, C. Graeff, and M. Stutzmann (unpublished).
[23] W. J. P. van Enckevort and E. H. Versteegen, J. Phys. Condens. Matter **4**, 2361 (1992).
[24] R. M. Chrenko, H. M. Strong, and R. E. Tuft, Philos. Mag. **23**, 313 (1971).
[25] G. Davies, Chem. Phys. Carbon **13**, 1 (1977).
[26] P. Denham, E. C. Lightowlers, and P. J. Dean, Phys. Rev. **161**, 762 (1967).
[27] H. B. Dyer, F. A. Raal, L. du Preez, and J. H. N. Loubser, Philos. Mag. **11**, 763 (1965).
[28] R. G. Farrer, Solid State Commun. **7**, 685 (1969).
[29] J. Walker, Rep. Prog. Phys. **42**, 1605 (1979).
[30] N. F. Mott and E. A. Davis, *Electronic Processes in Non-Crystalline Materials* (Clarendon, Oxford, 1971).
[31] H. Curtins and M. Favre, in *Amorphous Silicon and Related Materials* (World Scientific, Singapore, 1988).